# Evolution of Doppler Global Velocimetry Data Processing

**James F. Meyers**
**NASA Langley Research Center**
**Hampton, Virginia**

**Eighth International Symposium on Applications of Laser Techniques to Fluid Mechanics**
**July 8-11, 1996**
**Lisbon, Portugal**

# Evolution of Doppler Global Velocimetry Data Processing

James F. Meyers
NASA Langley Research Center
Hampton, Virginia
United States

## Abstract

The development of data processing techniques and algorithms for Doppler Global Velocimetry is presented. The discussion begins with the fundamental calculation of the velocity dependent transfer function of Iodine vapor, and proceeds through laboratory and wind tunnel investigations to develop insight into the physics of the technique. The knowledge gained through this process provided the basis for the development of algorithms to correct for optical distortions, electronic noise, and camera misalignment.

## Introduction

For the past six years, Doppler Global Velocimetry (DGV) has been under development at the NASA Langley Research Center. This technology can provide three-component velocity measurements of a flow as it passes through a selected measurement plane defined by a laser light sheet. Its ability to measure velocity within broad areas of the flow field, while maintaining cubic millimeter spatial resolutions in large wind tunnels, is of great interest to NASA. The increased productivity provided by DGV helps reduce the cost of aerodynamic testing. It is also an ideal measurement technology for validation of Computational Fluid Dynamics since it is capable of providing measurement grids equivalent to the computational grids. Further, the use of video technology provides real-time quick-look capability to view the velocity field as run conditions are changed, allowing adjustment of test parameters to optimize flow field conditions.

Although the basic principles were very simple, implementation of DGV technology as a flow diagnostics tool for routine wind tunnel application has proven somewhat difficult. Early investigations confirmed that an optical absorption line in Iodine vapor could be used to obtain images with velocity dependent amplitudes. However, it was also apparent that the images did not have sufficient quality to provide quantitative data

with acceptable accuracy. The effort to enhance this technology and develop a usable system with acceptable measurement accuracy has included wind tunnel investigations along with laboratory studies. The five year program has included velocities ranging from low subsonic to Mach 4.6, in various wind tunnels from the 1-x 1-meter Basic Aerodynamic Research Tunnel at Langley to the 40-x 80-foot National Subsonic Tunnel at NASA Ames. Although the basic optical hardware configuration has changed little, the data processing algorithms have undergone considerable development. The following is a description of that evolution along with example results from the various test programs.

## The Beginning

Komine, reference 1, devised Doppler Global Velocimetry when he used the light absorption characteristics of Iodine vapor to determine the absolute frequency of Doppler shifted laser light scattered by small particles passing through an Argon ion laser beam. This concept was a spin-off of his work with laser spectroscopy where an Iodine vapor cell was used in a feedback loop to stabilize the optical frequency of an Argon ion laser operating at 514.5 nm. The cell was used as the sensor in the feedback loop since the Iodine vapor transfer function provided optical frequency discrimination. The transfer function was found by passing a small portion of the laser beam through the cell, and determining the ratio of laser powers before and after the cell. By monitoring the power ratio while frequency tuning the laser, the characteristics of the absorption line were determined, figure 1. The laser frequency was then tuned to a point midway along the side of the absorption line, figure 1, and the laser power ratio electronically monitored. If the laser frequency, and thus the power ratio, changed, the feedback electronics adjusted the laser etalon temperature, and thus its length, to return the laser frequency to the set value. This principle, in an open loop version, was fundamental to the concept behind Doppler Global Velocimetry. With the laser frequency tuned to the midpoint of the absorption line as above, Doppler shifted scattered light would pass through the Iodine vapor with greater (or less, depending on the direction of the Doppler shift) absorption, thus establishing a fundamental relationship between the scattered light power ratio and velocity.

The implementation of this new technology uncovered characteristics that would make Doppler Global Velocimetry a uniquely capable flow diagnostic measurement system. Unlike other laser velocimetry systems, this technology did not require the optical resolution of individual seeding particles, since the velocity measurement was based on the fraction of collected scattered light absorbed by the Iodine vapor.

Thus, the source of the scattered light was immaterial. Further, the direct measure of optical frequency eliminated the problems of signal interference from multiple scatterers inherent in standard laser velocimetry. These characteristics allowed the laser beam to be expanded into a light sheet, and the laser power detectors replaced with Charge Coupled Device (CCD) video cameras, figure 2. In this configuration, each pixel element of the CCD became, in effect, a single detector collecting scattered light originating from the small volume within the light sheet imaged on that pixel. The ratio of the video output signals from the two cameras yielded images whose amplitude information was directly related to velocity.

These concepts were first demonstrated in the laboratory by Komine, *et al* at the Northrop Research and Technology Center, reference 2. Further development at the NASA Langley Research Center resulted in the first wind tunnel measurements, references 3 and 4. Additional studies at Northrop, under contract to NASA, found that a pulsed, injection seeded, frequency doubled Nd:YAG laser could be used as the laser source to obtain instantaneous velocity flow field mappings, reference 5.

## On to the Data Images

Since the optical frequency dependent transfer function imposed by the Iodine vapor was obtained by dividing the output (signal camera) image by the input (reference camera) image, figure 3, data processing was expected to be straight forward. Both the Northrop, references 2 and 5, and NASA, reference 3, efforts used analog dividers to normalize the RS-170 signal camera output with the reference camera signal as the images were transmitted from their respective cameras. Although the normalized images of a small supersonic jet, reference 2, and the vortical flow above a delta wing, reference 3 and figure 4, showed the expected velocity dependencies, the images were very noisy and the velocity structures were not well defined.

### Phase I – Image Alignment

A laboratory investigation was conducted at NASA to determine the reason for the noise and poorly defined images. A test target, figure 5, was viewed by the receiver optical system and the cameras carefully aligned to overlap the pixels. If the alignment was perfect, the normalized image would be a flat gray since the transfer function remained constant throughout the image. Unfortunately, the edges of the dots on the test target were clearly visible with overall patterns

indicative of optical differences between the signal and reference optical paths, figure 6. Adjusting camera position, pan, tilt, and magnification improved the normalized image, but perfect alignment was never achieved. The inability to obtain the proper alignment was traced to minor imperfections in the receiver optical elements. One potential solution was to replace the optics with components built to tighter specifications. However, a more cost effective solution was to remove the distortions using image processing techniques. After using the analog circuitry to obtain the best physical alignment, the electronics were disconnected and the signal and reference images acquired by computer in sequence by a video frame grabber. Since the target was composed of a grid of evenly spaced dots, dewarping algorithms in a commercial software package were used to remove the distortions. While the resulting dewarped images appeared to be square, the normalized image still showed the dot edges, indicating that the distortions were not totally removed. Further investigation found that the commercial packages could remove linear variations such as perspective, but were incapable of removing the effects of minor nonlinear distortions originating from optical imperfections in the receiver optics. These packages used a single first, second or third order equation to describe the entire horizontal and vertical directions respectively. While this process might be acceptable for visual applications, it was inadequate for image normalization.

Since the laboratory investigation identified minor optical imperfections as a cause of measurement error, and the commercial image processing software provided insight into a potential solution, a development program to obtain the needed image processing algorithms was undertaken. The resulting method was to use piecewise, bilinear warping procedures to subdivide the target image into sections sufficiently small to correct for the minor optical distortions, reference 4. In practice, a grid of 20 by 20 sections, defined by the dot centroids in the test target, appeared to yield sufficient correction. Dewarping figure 5 with this method yielded figure 7. An improvement in image alignment was found when the dewarped images were normalized, figure 8.

## Phase II – Noise Reduction

The vortical flow field above the delta wing was again measured, and the acquired images dewarped before normalization, reference 4. Additionally, the Gaussian intensity profile of the light sheet was flattened to lessen occurrences of pixel saturation in the center of the light sheet and insufficient scattered light at the edges. The flat intensity profile was obtained by replacing the cylindrical lens with a

high-speed galvanometer scanner. Scattering angle and polarization dependent Mie scattering intensity variations were also reduced by placing a quarter-wave plate in the laser output optical path to circularize the laser light polarization, reference 7.

Although aerodynamic symmetry was not present, as shown by laser light sheet flow visualization in figure 9, the normal and burst vortical flow field above the delta wing was clearly detected, figure 10. In spite of the vast improvement in the data image, it was still noisy and contained unrealistic values at the edges of the smoke plume. An analysis of CCD video camera operation revealed several characteristics that could be responsible for these anomalies. These characteristics included dark current, variations in pixel sensitivity, charge transfer noise, modulation transfer function, and field interlacing. The characteristics, the effects on the data image, and the correcting procedures are described below:

Dark current - CCD video cameras, in the manner of other photo-electronic detector systems, occasionally produce spurious photoelectrons without the stimulation of triggering photons. The collected charge represents an offset in the pixel amplitude that must be removed before normalization calculations are performed to determine the correct Iodine vapor transfer function.

Variations in pixel sensitivity - Minor imperfections in the photo-electronic sensor result in variations of pixel-to-pixel quantum efficiency. The effect is random noise superimposed on the acquired image. Since the quantum efficiency is constant, the pixel-to-pixel variations can be removed through calibration of pixel sensitivity. The calibration is typically obtained by illuminating the CCD sensor with flat field light at two intensities, and determining the sensitivity slope or quantum efficiency for each pixel. Flattening the CCD sensitivity response then consists of simply multiplying the data images by the average quantum efficiency divided by the quantum efficiency for each respective pixel.

Charge transfer noise - Once the photoelectrons have been acquired during field acquisition, the field image is transferred from the CCD by moving the charge packets from capacitor to capacitor until they reach the output port. As each charge packet leaves a capacitor, there is a possibility that one or more electrons may be left behind, or electrons left by previous packets, added. These random charge variations become a white noise component in the output signal, and thus a superimposed random noise on the acquired image. The best method to reduce the effect of charge transfer noise is to low pass filter the image by convolving the image with a 5x5 top hat kernel. Since this kernel

matches the measured modulation transfer function of the camera system, only high frequency charge transfer noise is removed, while the data information is maintained. With industry standard RS-170 video cameras, the remaining noise is estimated to be 1-percent of full scale, or a velocity uncertainty of ±2 m/sec.

Modulation Transfer Function - The Modulation Transfer Function (MTF) is a measure of spatial frequency limit or sharpness factor of the imaging optics and CCD camera. For example, a photograph taken with an f16 lens opening produces a sharper image than the same photograph taken with an f2 lens opening. The MTF of a CCD video camera is related to electronic charge leakage between adjacent pixels. The combined lens/camera MTF is measured by imaging a spatial step change in light intensity, and determining the kernel needed to match the measured response. A typical industry standard RS-170 video camera has an MTF that matches a 5x5 top hat kernel.

Field interlacing - Industry standard RS-170 video cameras are interlaced devices which acquire photons in the even pixel rows while transferring the previously acquired image in the odd pixel rows out of the camera. During the next acquisition cycle, the newly acquired even row image is transferred out while the odd rows acquire the next image. Standard video devices reconstruct the video frame by combining the two interlaced images. Since the interlaced or field images are acquired at different times, motion within the viewed scene adds distortion to the combined image. This effect can be seen as a series of horizontal lines that indicate a change of scattered light caused by variations in the smoke cloud and/or a change in the velocity flow field occurring between the acquisition of the two video fields. Thus the two fields are separated and the missing rows interpolated to yield a field image that is then dewarped and processed.

Calibrations and procedures were developed to account for the CCD video camera characteristics outlined above. Dark current images were acquired and saved for use during data processing. Each video camera system, including video amplifiers, signal processing electronics, and computer frame grabber, were calibrated for pixel sensitivity. The MTF for each camera was determined and found to be equivalent to a 5x5 kernel. Finally, data processing algorithms were developed to subtract dark current contributions from the data images, flatten the effects of pixel sensitivity variations, low pass filter the data images, and separate the video fields and interpolate the missing rows.

## Phase III – Optical Difficulties

Following completion of the data processing software, the DGV system was installed in the Langley Unitary Plan Wind Tunnel and used to investigate the vortical flow above a delta wing at Mach 2.8. This investigation presented the opportunity to determine the measurement characteristics from submicron diameter water condensation particles. The uniform illumination, shown in the photograph of the laser light sheet visualization in figure 11, eliminated potential measurement uncertainties related to variations in smoke density. The visualization showed three distinct scattered light intensity levels: free stream, behind the cross flow shock, and the vortex. The velocity image, figure 12, did not yield the expected change in velocity at the intensity boundaries. This anomaly was traced to the inclusion of background light in both the signal and reference images. The background light level included contributions from the camera dark current discussed above, reflected laser radiation from tunnel and model surfaces, and ambient lights. The influence of ambient light was reduced by placing a green photographic filter in front of each camera. The remaining background light was measured by acquiring images under run conditions, but without particles in the flow. These background images were then subtracted from the signal and reference data images, respectively, prior to normalization.

Closer examination of the measured velocity images revealed unexpected velocity patterns, especially in the constant velocity free stream portion of the image. Since the condensation scattered light in a uniform manner, the origins of the velocity patterns were traced to the receiver optical system. An overall velocity bias was found to originate from a mismatch in optical transmission between the signal and reference paths. The transmission differences were caused by the characteristics of the beamsplitter, windows in the Iodine vapor cell, neutral density loss through the Iodine vapor, and mismatch in electronic signal amplification. Spatially dependent biases were caused by dirt on the optics, bending of the beamsplitter and Iodine vapor cell windows, and polarization effects from the interaction of Mie scattered laser light with the beamsplitter. The bias and spatially dependent transmission effects were isolated by adjusting the laser output frequency to place the Doppler shifted frequency outside the Iodine absorption line and acquiring data normally. The resulting normalized images were inverted and averaged to obtain a transmission correction image for multiplication with the normalized data images prior to velocity conversion.

## Moving to the Third Dimension

Although the several wind tunnel investigations using the single-component DGV, reference 6, provided insight into various aerodynamic flows, the primary interest of aerodynamicists was three-component velocity measurements in standard $U$, $V$, and $W$ component directions. Two receiver optical systems were added to the DGV system and laboratory tests conducted on a rotating wheel to develop three component measurement capability.

### Phase I – The Laboratory

The three-component DGV optical system was placed about a rotating wheel, with a receiver set on the left, right and above with a 30° angle to the plane of the wheel. The wheel was illuminated with a cone of laser light propagating in the horizontal plane, and inclined by 45° to the wheel. The view from each receiver of the calibration card is shown in figure 13. The perspective and optical distortions were removed using the normal piecewise bilinear warping software. The number of rows and columns extending from the central dot were matched for the three images. The resulting warped views are also shown in figure 13. Thus, the images had the proper overlay to not only determine the $A$, $B$, and $C$ velocity components, but also determine the standard $U$, $V$, and $W$ velocity components using triangulation procedures for each pixel location.

The wheel was spun and the velocity data acquired. The measured and converted velocity images are shown in figure 14. As expected, the $U$ component was nominally 0 m/sec, and the $V$ and $W$ components had the appropriate profiles for a solid body of revolution, with the proper 90° phase difference between components.

### Phase II – The Tunnel Test

The first wind tunnel application of three-component DGV served as a demonstration of the Langley-designed system for the 40-x 80-foot National Subsonic Wind Tunnel at the NASA Ames Research Center, reference 8. The system orientation for the measurement of the jet flow exiting from a High Speed Civil Transport engine model is shown in figure 15. The investigation yielded resolved $U$, $V$, and $W$ velocity components of a 0.22 m diameter jet, operating at temperatures up to 700° C with velocities over 500 m/sec. An example image, figure 16, of the streamwise velocity component obtained within a plane normal to the jet axis, 0.25 jet diameters downstream from the exit, clearly shows

the velocity deficit caused by the conical central body. The spatial measurement grid capability of the technique, even at focal distances up to 15.5 m, is shown by the X-Y plot of the measured velocities obtained from a single row of pixels, with a resolution of 1.25 mm, along the diameter of the jet.

This investigation revealed two additional problems. Vibration in large wind tunnels, coupled with the need for long focal distances, placed unrealistic requirements on the maintenance of optical alignment. The other concern was the large measurement uncertainty at the edge of the smoke. As with earlier obstacles, system misalignments that occurred during wind tunnel testing were corrected using image processing techniques. The dewarped signal and reference images were cross correlated to determine their spatial misalignment. The signal image was then shifted to realign the two images before normalization. The reference images from each component were also cross correlated to determine their spatial misalignment. Again, two components were shifted to align the images before conversion to the standard $U$, $V$, and $W$ velocity components. It is noted that only the reference images were correlated to insure the absence of velocity dependencies induced in the signal images by the Iodine vapor that would influence the correlation results.

As the smoke density dissipated at the edge of the plume, the acquired signal and reference amplitudes decreased, thus increasing the uncertainty of the corresponding normalized results. Additionally, since the plume moved and changed with time, reduced scattered light levels influenced a greater spatial area when sequential velocity images were averaged, thus increasing overall measurement uncertainty. By raising the acceptable threshold levels, measurement uncertainties were reduced. Additionally, a band of four pixels along the smoke plume edges was removed in each normalized image to negate the low frequency rolloff induced by the spatial low pass filter described above.

## The Current Technology

Wind tunnel entries continued with the three-component investigation of a wing tip vortex, and its interaction with a trailing model in the Langley 30-x 60-foot Full Scale Wind Tunnel, figure 17. Although this facility was smaller than the NASA Ames 40-x 80-foot National Subsonic Wind Tunnel, it had an open test section making installation of the optics more difficult. Two of the receiving optical systems were installed in pods placed on the test section floor, figure 17, at focal distances of 7.5 m, and the third was placed on top of the test section inlet at a focal distance of 18.25 m. The 5-cm diameter vortical flow was

measured with the upstream airfoil set to 2- and 10-degree angles of attack. Averaging the cross-flow velocity data images produced the results shown in figure 18. While these images gave an indication of the vortex motion, they provided little information about the vortex structure. Using the cross correlation procedure described above, the vortex structures became clear, figure 19.

The latest entry was the investigation of the flow entering a powered helicopter model tail rotor in the 14-x 22-foot Subsonic Tunnel. The three velocity components indicated that the flow moved downward at 45 degrees in a uniform manner, figure 20. The measurements showed the influence of the main rotor flow, but the expected rotor tip vortices were not found. The lack of evidence from tip vortex passage was traced to flow field averaging by the video cameras. During the 17 msec video field acquisition of scattered light, the main rotor rotated 240 degrees which moved at least two vortices through the light sheet. Further complications included the comparatively large measurement uncertainty, ±2 m/sec, attributed to charge transfer noise, and the inability to maintain a constant temperature in the Iodine vapor cells because of the -5° C ambient temperature.

The implications of these investigations have led to major modifications in the current DGV optical system. These modifications will increase measurement capabilities along with measurement accuracy. The Argon ion laser is being replaced with a pulsed single-frequency, frequency-doubled Nd:YAG laser to provide the capability to measure unsteady flow fields. Further, the 10 nsec pulse width will provide measurement images with full turbulent bandwidth allowing the measurement of turbulence intensity and turbulence power spectra using spatial domain techniques. The industry standard RS-170 video cameras are being replaced with 10-bit digital cameras to increase velocity measurement resolution. The remaining modification is the enclosure of each Iodine vapor cell in an insulated container to provide better temperature stability. All Iodine vapor cell stem and body temperatures are measured for each set of three-component data images acquired. These temperatures are then used to theoretically determine the Iodine vapor cell transfer function for each corresponding data image. This yields greater measurement accuracy than would be obtained using calibrated transfer functions for a few selected temperatures.

## Concluding Remarks

The development program conducted at NASA Langley Research Center has shown that Doppler Global Velocimetry is a robust and versatile

technology that can provide global three-component velocity measurements of an aerodynamic flow. Its evolution included laboratory and wind tunnel testing to develop a basic understanding of the technology, the nature of Mie scattered light, and the characteristics of the elements comprising the DGV system. Example test results were presented and characteristics identified which triggered advances in data processing algorithms. The results also showed a progressive improvement in data quality as the new algorithms were included during processing. The measurement envelope increased during the development program from single-component measurements of low-speed flows in a small wind tunnel to the measure of a Mach 2.8 flow using submicron water condensation, and three-component investigations of a 22-cm diameter hot jet in a 40–x 80–foot wind tunnel and a 5-cm diameter tip vortex measured at a focal distance of 18.25 m.

## References


1. Komine, H.: *System for Measuring Velocity Field of Fluid Flow Utilizing a Laser -Doppler Spectral Image Converter*, US Patent 4 919 536, 1990.

2. Komine, H.; Brosnan, S. J.; Litton, A. B.; and Stappaerts, E. A.: *Real-time Doppler Global Velocimetry*, AIAA 29th Aerospace Sciences Meeting, Reno, NV, paper 91-0337, January 7-10, 1991.

3. Meyers, J. F.: *Review of Typical Applications - Wind Tunnels*, von Karman Institute for Fluid Dynamics, Lecture series 1991-08, Brussels, Belgium, Laser Velocimetry, June 10-14, 1991.

4. Meyers, J. F.: *Doppler Global Velocimetry – The Next Generation?*, AIAA 17th Aerospace Ground Testing Conference, Nashville, TN, Paper 92-3897, July 6-8, 1992.

5. Komine, H.; Brosnan, S. J.; Long, W. H.; and Stappaerts, E. A.: *Doppler Global Velocimetry Development of a Flight Research Instrumentation System for Application to Non-intrusive Measurements of the Flow Field*, NASA Report CR-191490, 1994.

6. Meyers, J. F.; Usry, J. W.; and Miller, L. S.: *Assessing the Capability of Doppler Global Velocimetry to Measure Vortical Flow Fields*, Journal of Aerospace Engineering, part G, vol 208, pp. 99-105, December 1994.

7. Mie, G.: *Optics of Turbid Media*, Ann. Phys. Vol 25, pp. 377-445, 1908.

8. Meyers, J. F.: *Development of Doppler Global Velocimetry for Wind Tunnel Testing*, AIAA 18th Aerospace Ground Testing Conference, Colorado Springs, CO, paper 94-2582, June 1994.

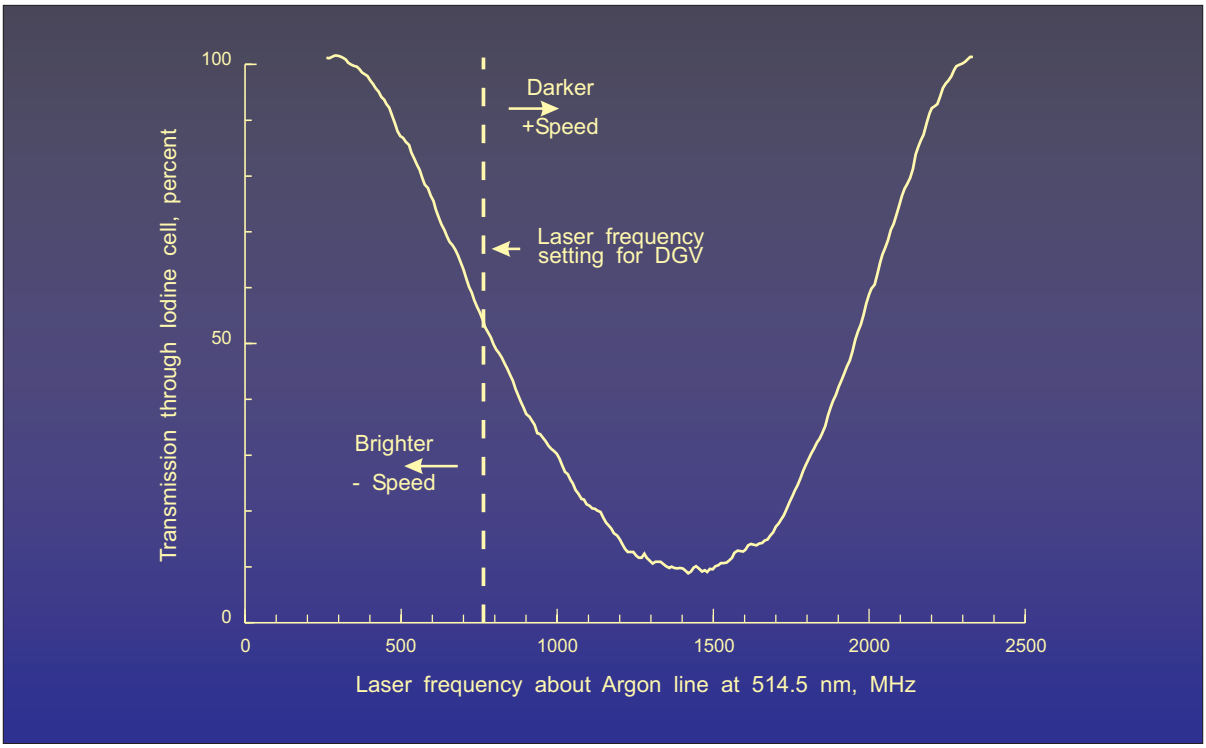


Figure 1.- Transfer function of the Iodine vapor cell.

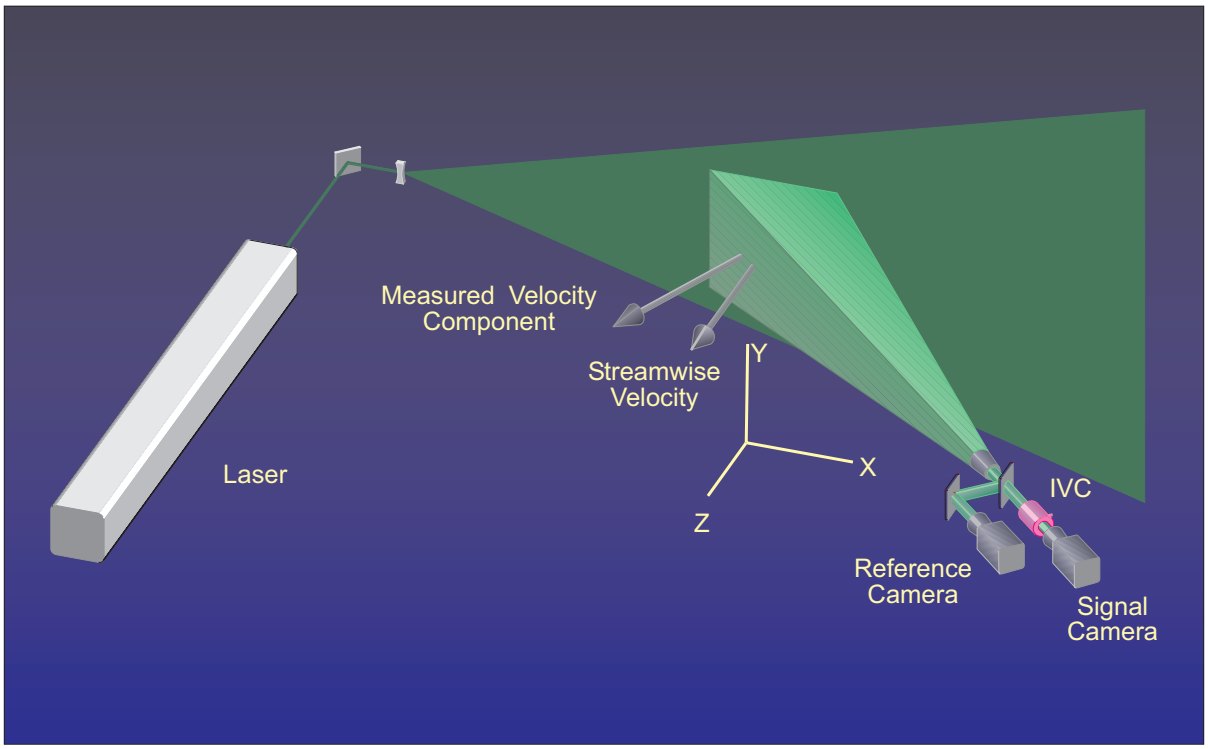


Figure 2.- Pictorial view of the Doppler Global Velocimeter used in the Basic Aerodynamics Research Tunnel to measure the flow above a 75° delta wing.

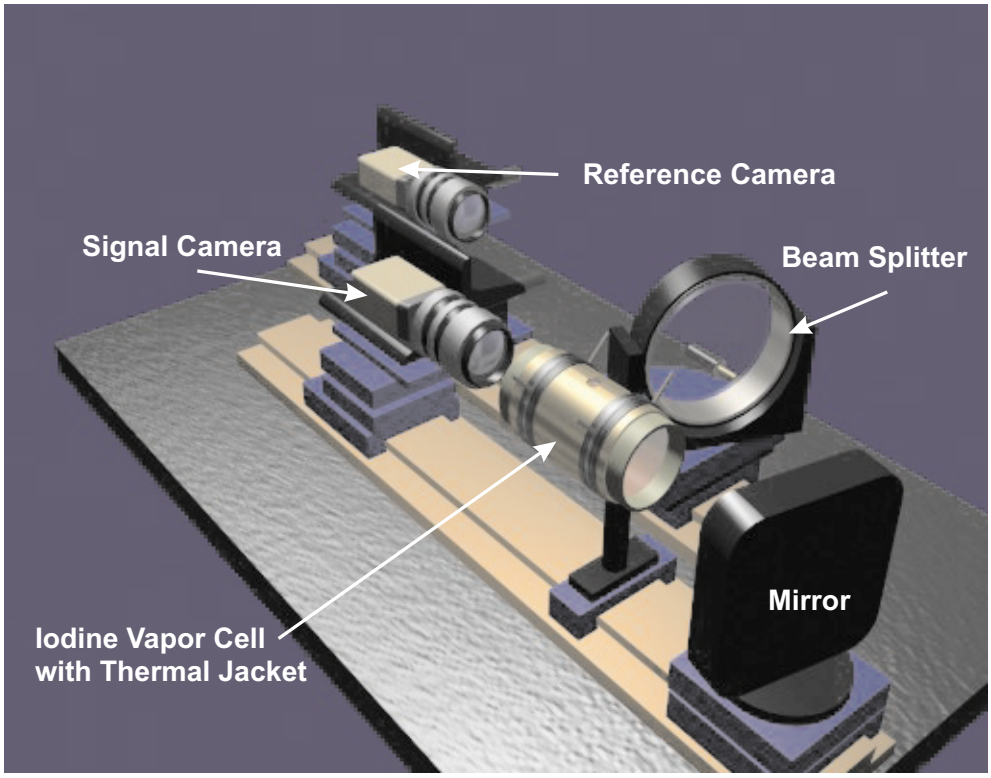


Figure 3.- Pictorial view of the receiver optical system.

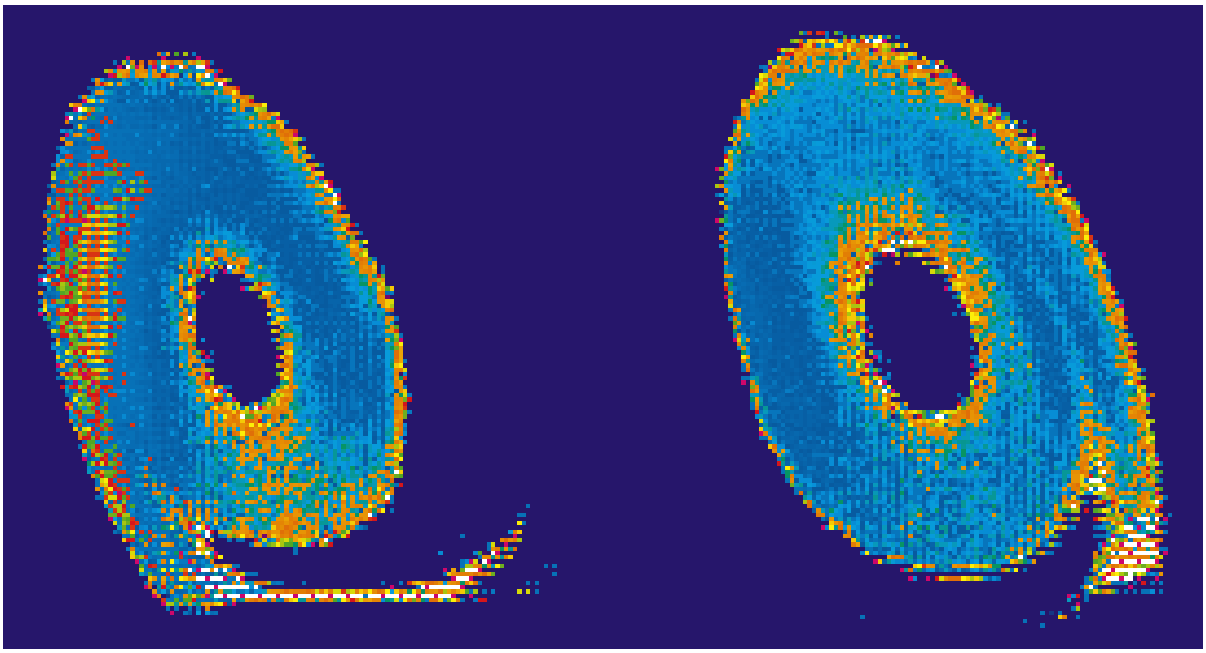

Figure 4.- DGV data image for the near cross-flow component of the vortical flow above a $75^{o}$ delta wing at an angle of attack of $20.5^{o}$.

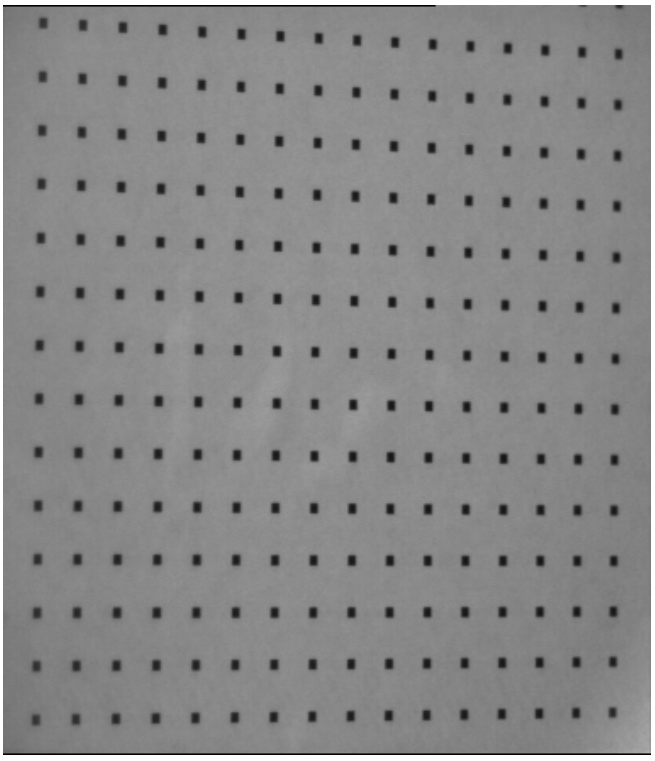

Figure 5.- View of equally spaced dots on a flat card placed in the laser light sheet position.

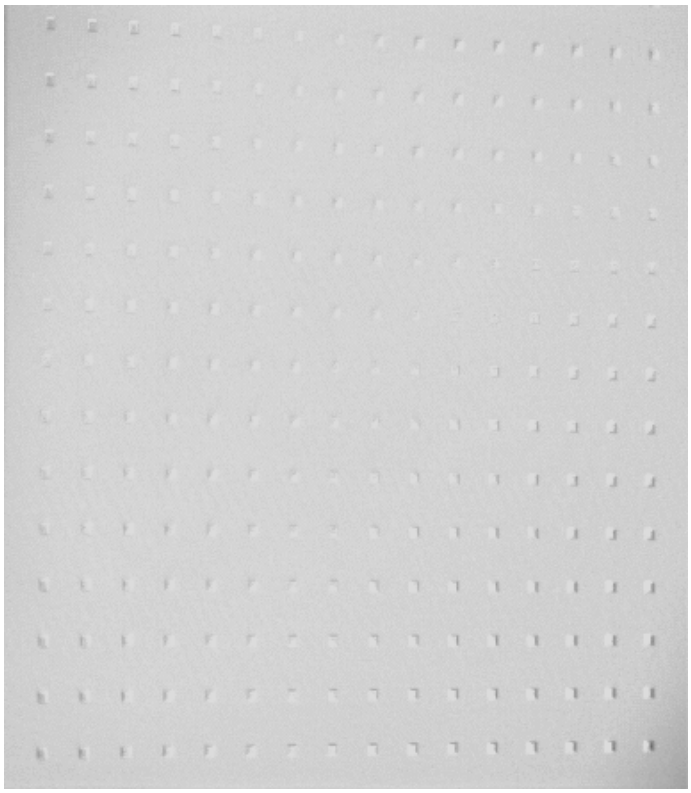

Figure 6.- Normalized image based on the dot card image shown in Figure 5.

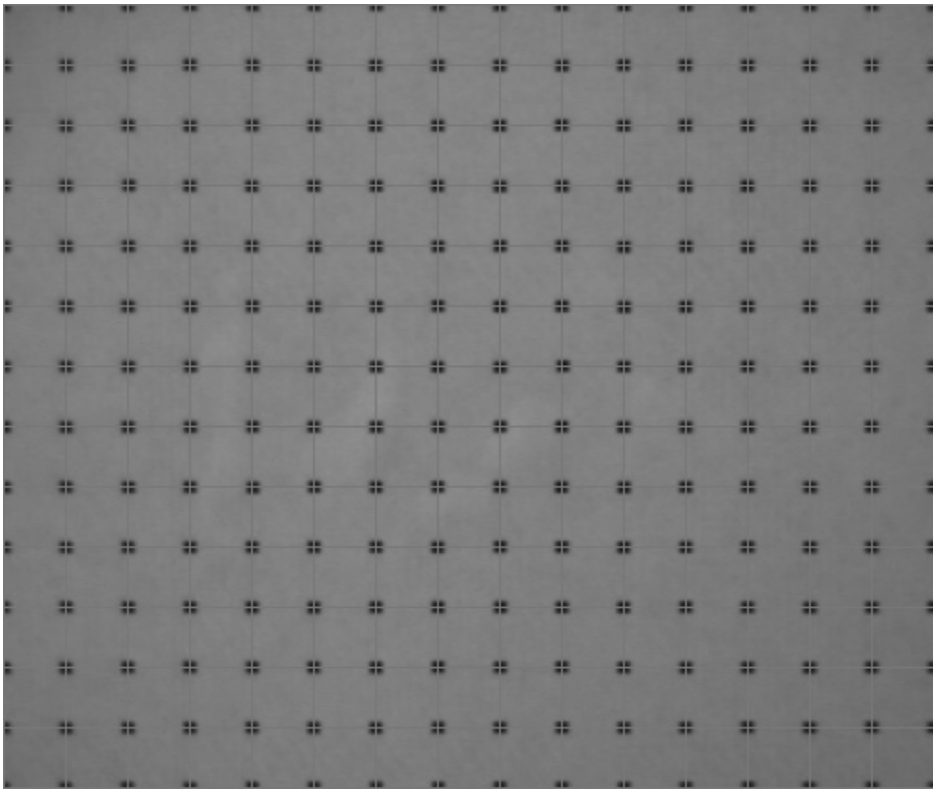

Figure 7.- Dewarped dot card image.

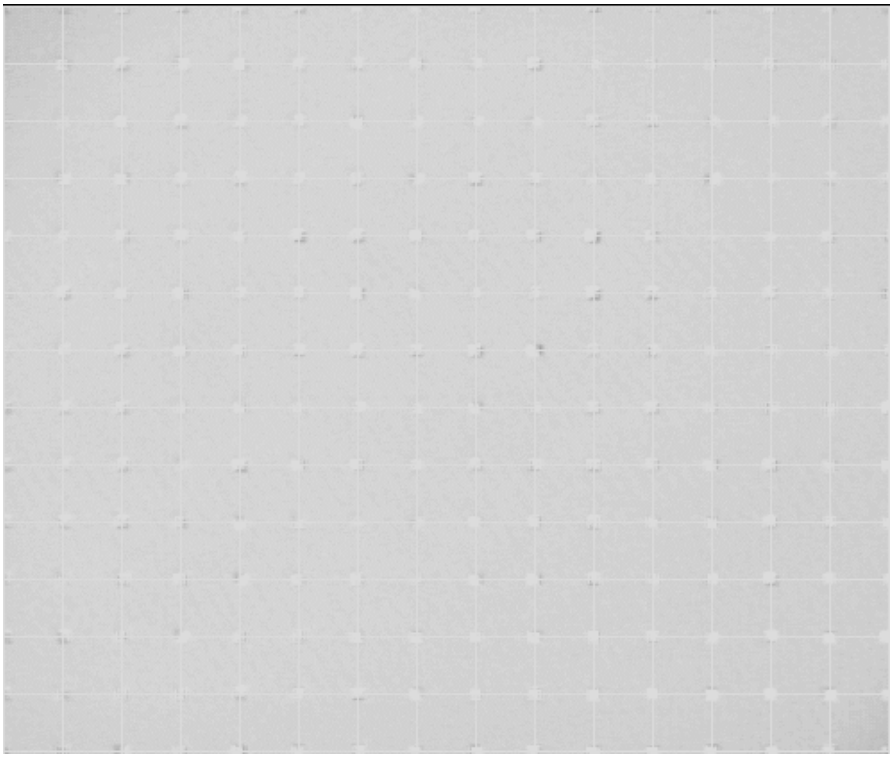

Figure 8.- Normalized image based on the dewarped dot card image shown in Figure 7.

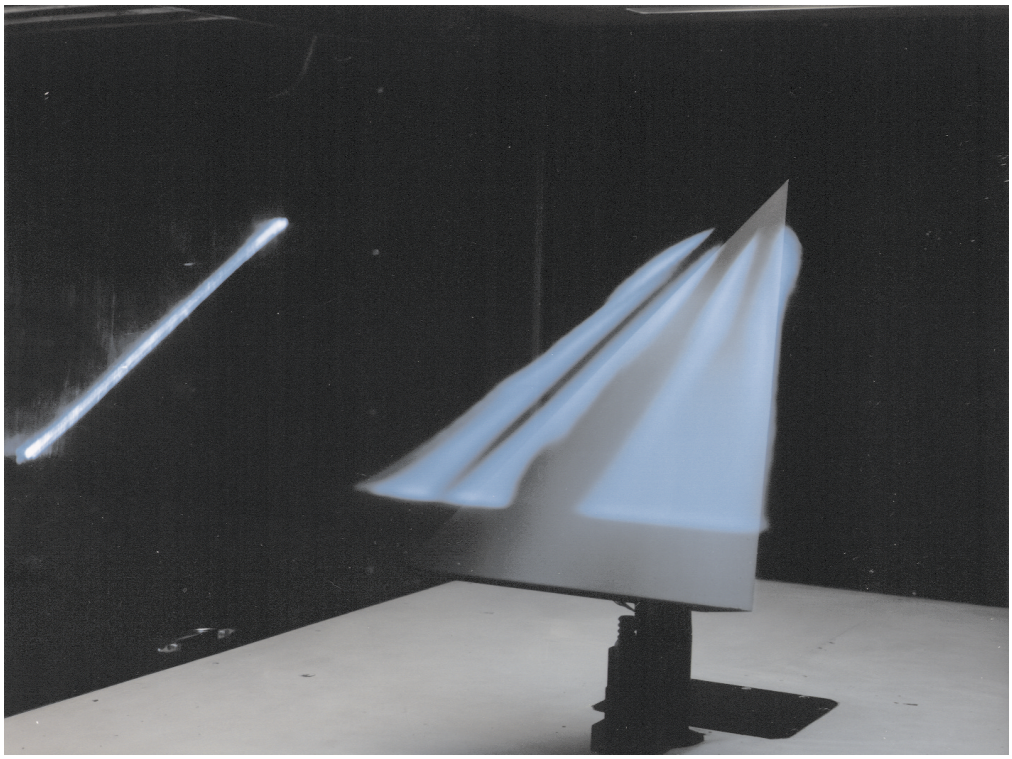

Figure 9.- Flow visualization of the vortical flow above a $75^{o}$ delta wing at an angle of attack of $20.5^{o}$.

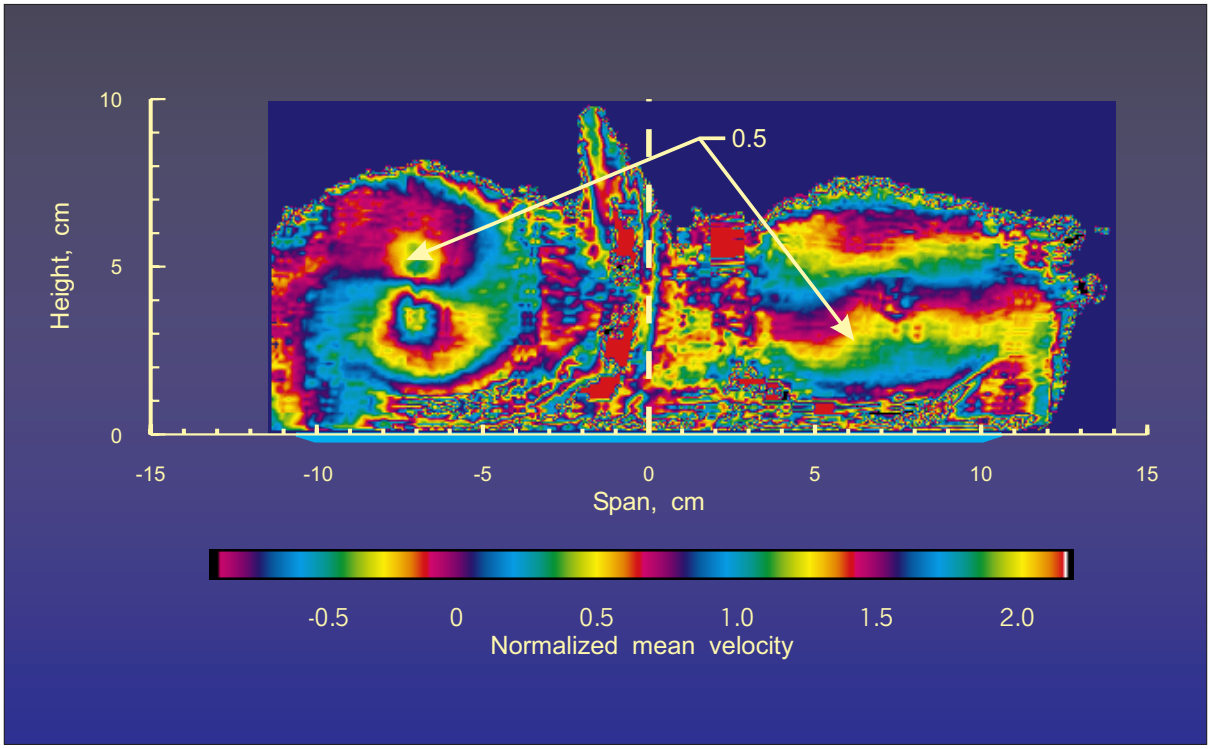


Figure 10.- DGV data image for the near cross-flow component of the vortical flow above a 75$^{o}$ delta wing at an angle of attack of 20.5 $^{o}$.

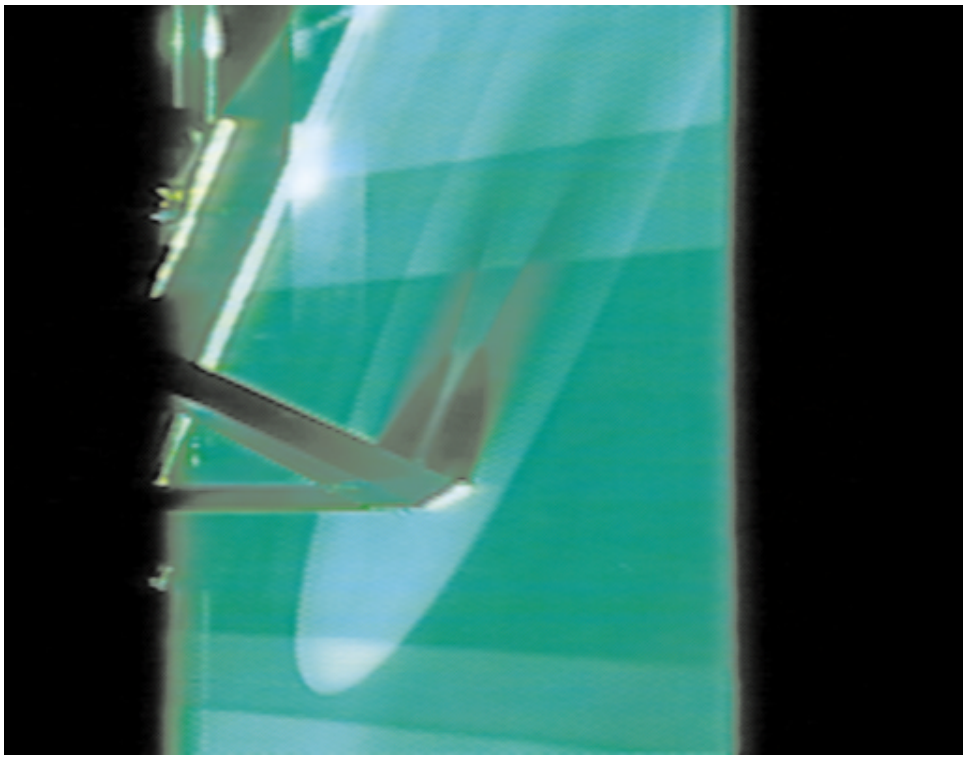

Figure 11.- Photograph of the laser light sheet above a 75$^{o}$ delta wing at the 95% chord location at Mach 2.8.

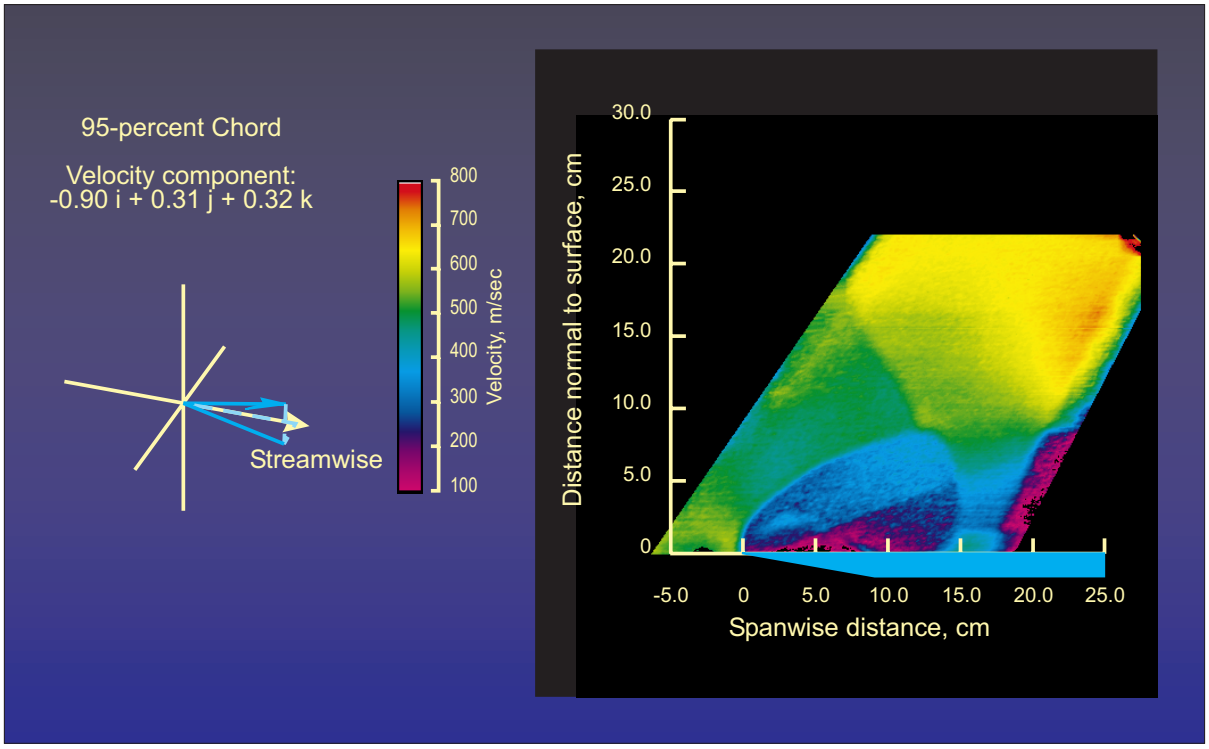


Figure 12.- Map of the velocity flow measured by the DGV system of the vortical flow above a 75$^{o}$ delta wing at the 95% chord location at Mach 2.8.

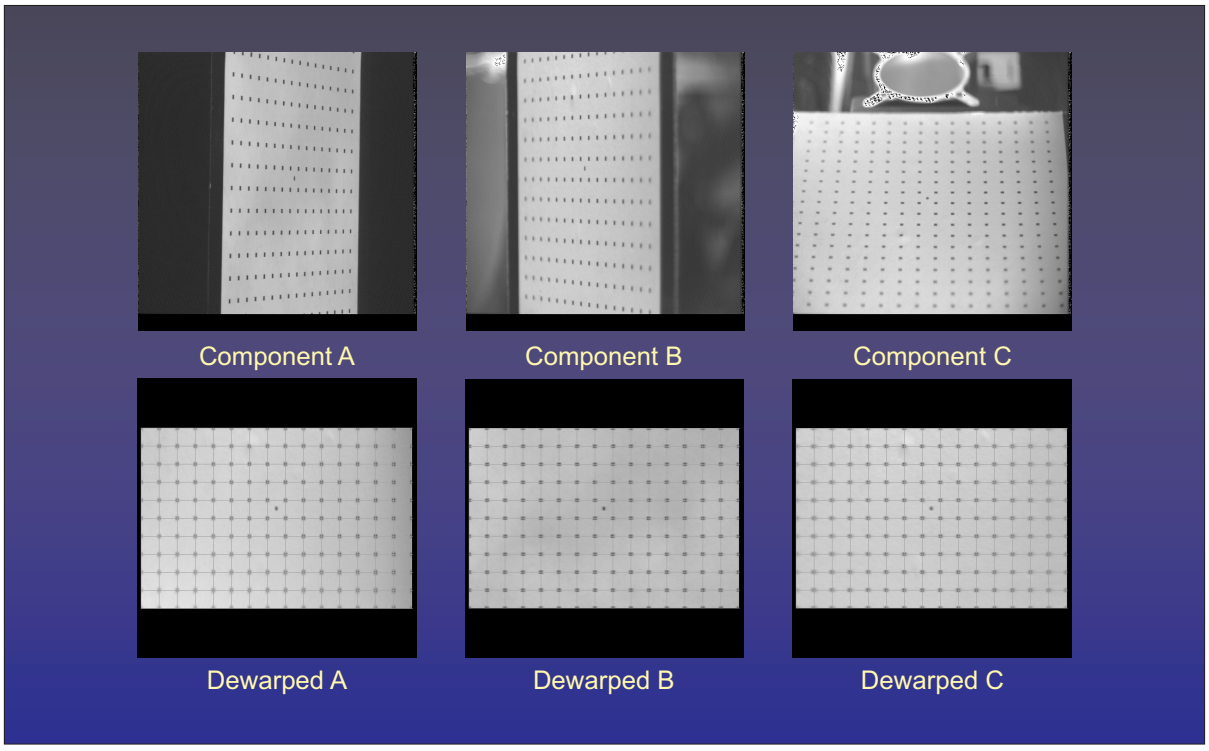


Figure 13.- Views of equally spaced dots on a flat card from the left, right, and above with an inclination of 30 $^{o}$ from the card plane before and after warping.

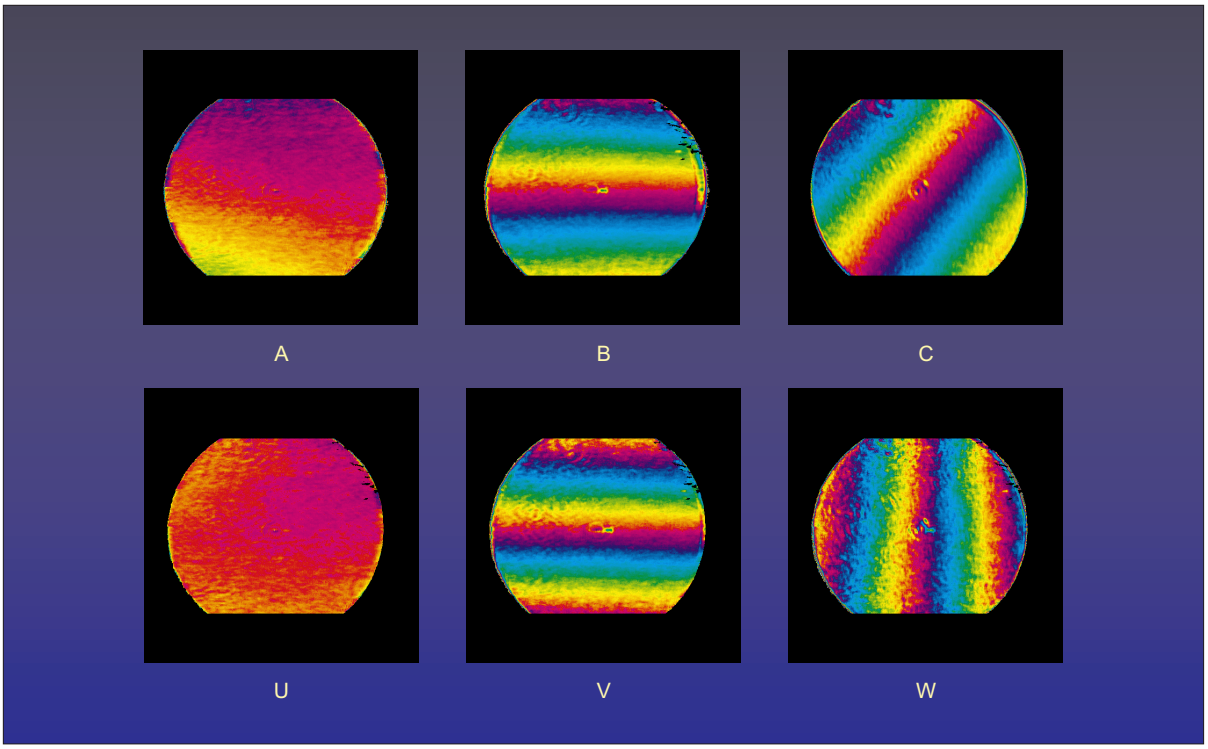


Figure 14.- Original and resolved U, V, and W velocity component images of a rotating wheel obtained from the three views shown in figure 13.

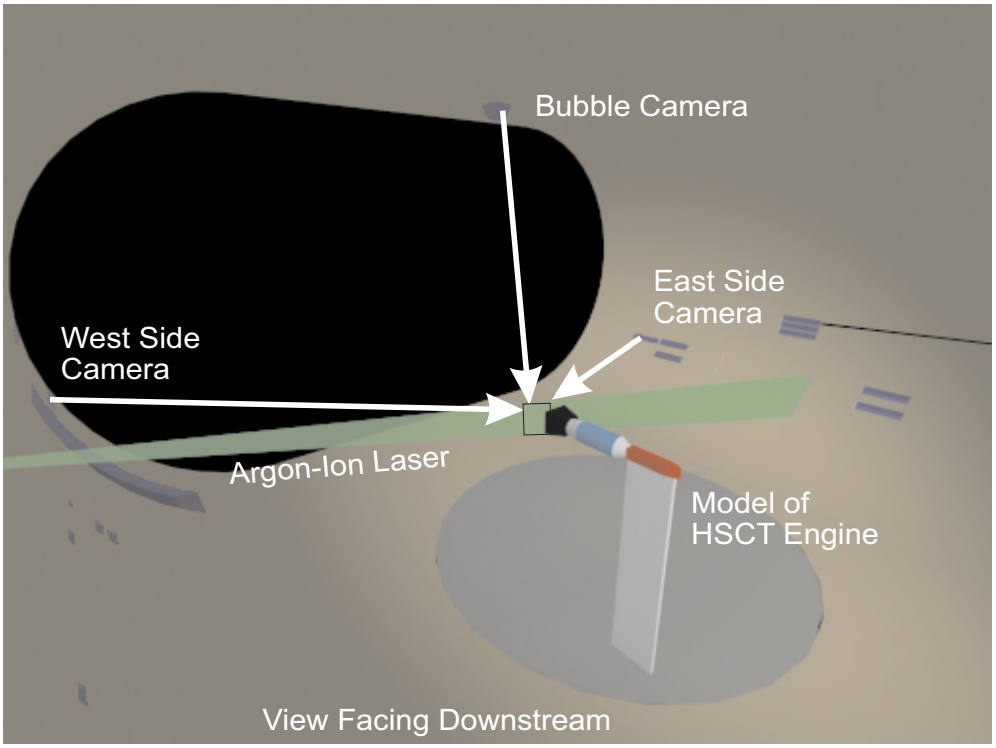


Figure 15.- Configuration of the three-component DGV optical system in the NASA Ames Research Center 40-x 80-foot National Subsonic Wind Tunnel to measure the flow from a high-speed jet.

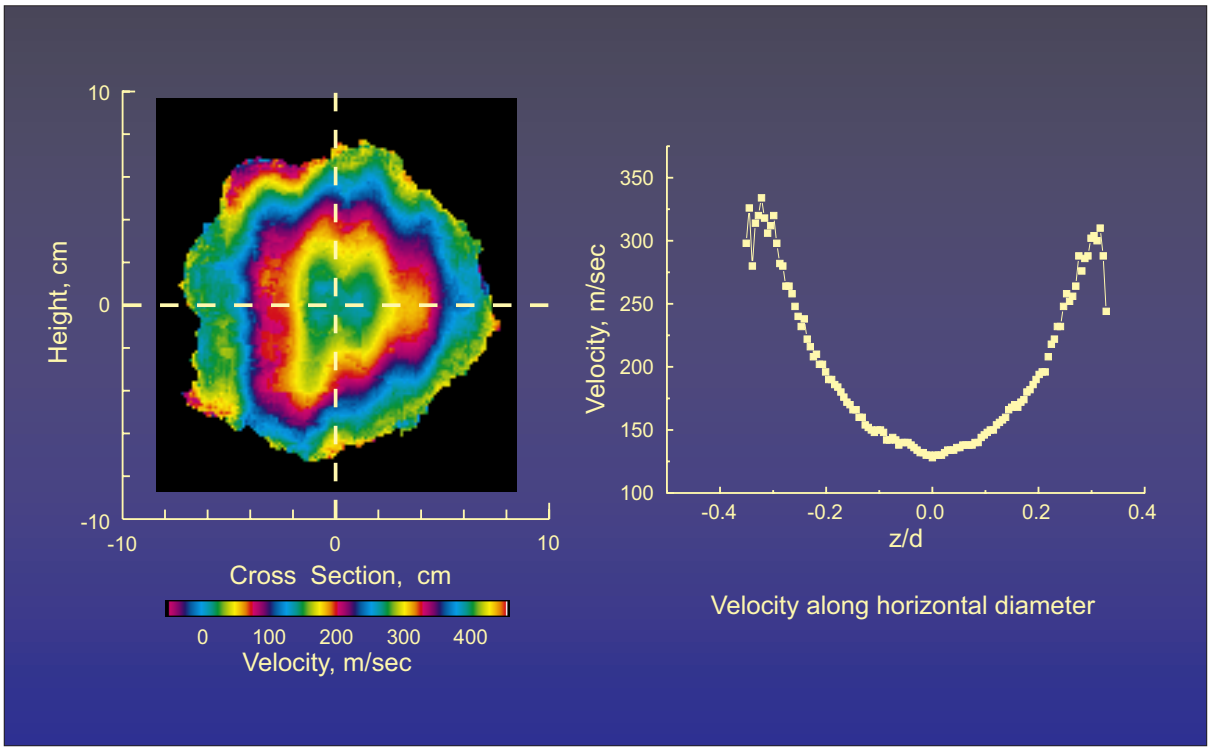


Figure 16.- Resolved streamwise component of velocity from the high-speed jet flow operating at 463$^{0}$ C at a free stream Mach number equal to 0.15.

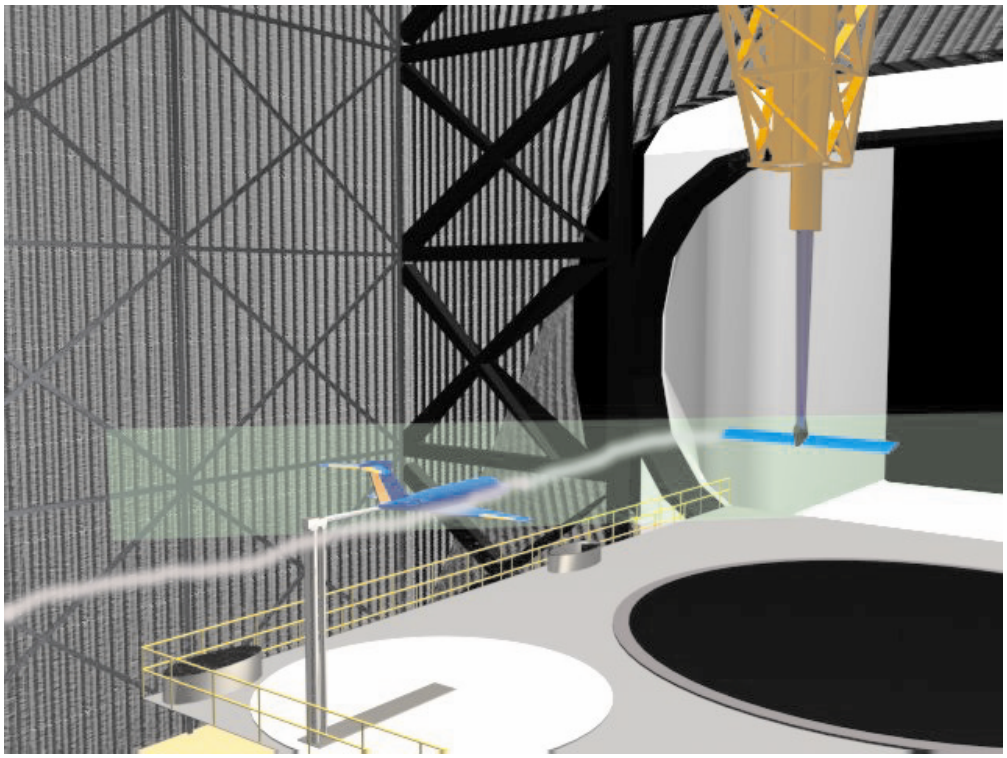

Figure 17.- Pictorial view of the wing tip vortex interaction investigation in the Langley 30-x 60-foot Full Scale Wind Tunnel.

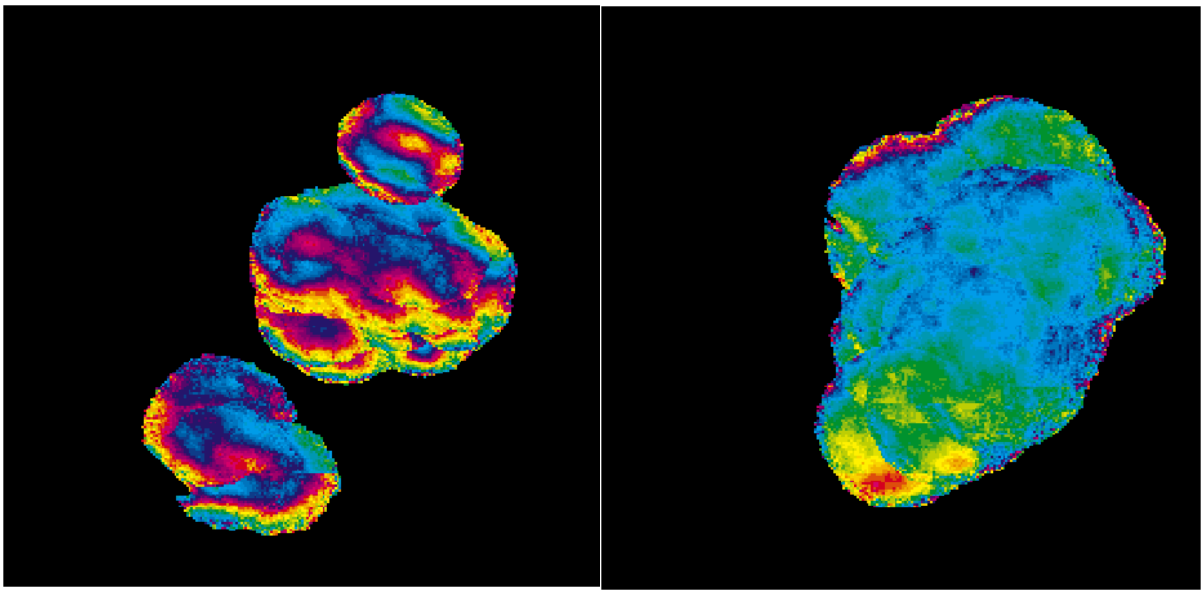

Angle of Attack: 2° 10°

Figure 18.- Cross flow component velocity mapping of the wing tip vortex, normal average.

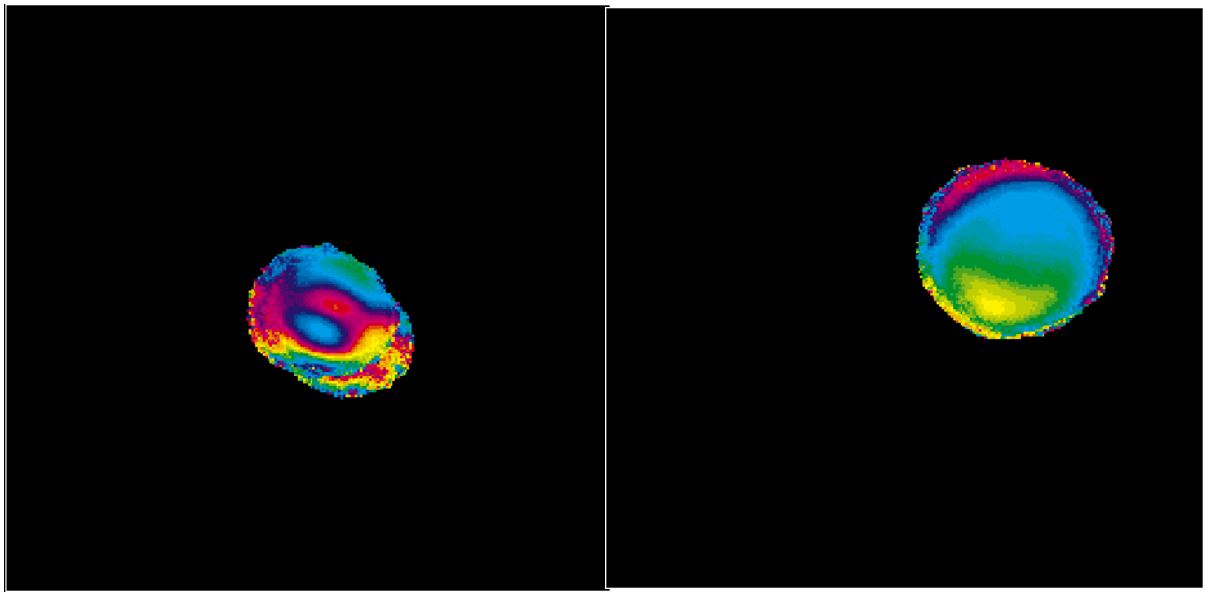

Angle of Attack: 2° 10°

Figure 19.- Cross flow component velocity mapping of the wing tip vortex, spatially correlated average.

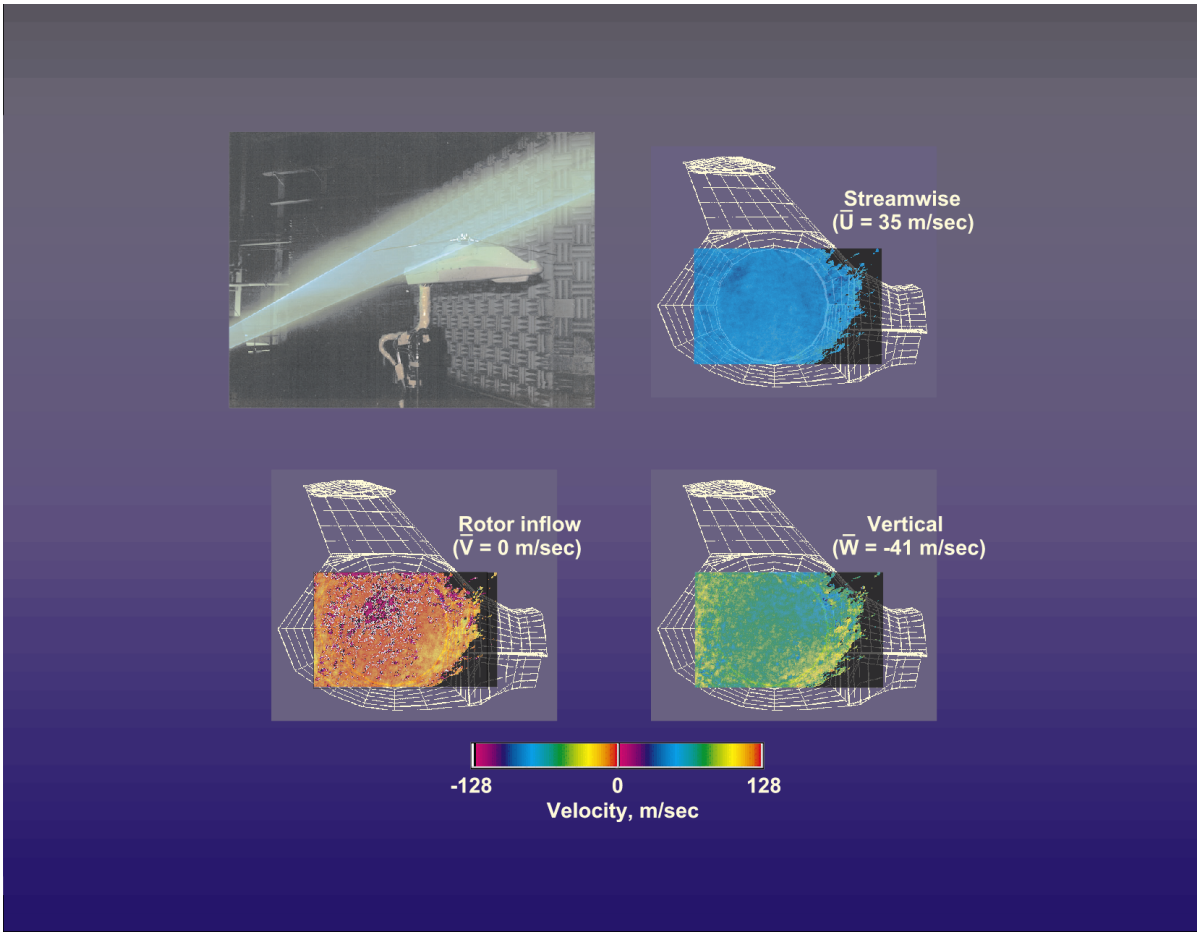


Figure 20.- Velocity measurements of the inflow to the tail rotor of a powered helicopter model in the 14-x 22-foot Subsonic Tunnel.